

RESEARCH ARTICLE

Channeling vorticity: modeling the filter-feeding mechanism in silver carp using μ CT and 3D PIV

Karly E. Cohen¹, L. Patricia Hernandez^{1,*}, Callie H. Crawford² and Brooke E. Flammang²

ABSTRACT

Invasive silver carp are thriving within eutrophic environments in the United States, in part because of their highly efficient filter-feeding mechanism. Silver carp utilize modified gill rakers to capture a specific range of food; however, their greatly modified filtering morphology allows them to feed on phytoplankton and zooplankton ranging in size from 4 to 85 μ m. The filtering apparatus of silver carp comprises rigid filtering plates where the outer anatomy of these plates is characterized by long parallel channels that change in orientation along the length of the plate. Here, we investigate the underlying morphology and concomitant hydrodynamics that support the filtration mechanisms of silver and bighead carp. Bighead carp are also invasive filter feeders, but their filtering apparatus is morphologically distinct from that of silver carp. Using 3D particle image velocimetry, we determined how particles and fluid interact with the surface of the gill rakers/plates. Filtering plates in silver carp induce strong directed vortical flow, whereas the filtering apparatus of bighead carp resulted in a type of haphazard cross-flow filtration. The organized vortical flow established by silver carp likely increased the number of interactions that the particle-filled water had with the filtering membrane. This strong vortical organization is maintained only at 0.75 body lengths s^{-1} , and vortical flow is poorly developed and maintained at slower and faster speeds. Moreover, we found that absolute vorticity magnitude in silver carp is an order of magnitude greater than in bighead carp.

KEY WORDS: Filter feeding, Particle image velocimetry, *Hypophthalmichthys molitrix*, Gill rakers

INTRODUCTION

Silver carp, *Hypophthalmichthys molitrix*, is a filter-feeding cyprinid from Eastern China and Siberia that is a major focus of aquaculture efforts worldwide and has proven to be highly invasive in the Mississippi River basin and other drainages in Europe, Asia and Africa (Solomon et al., 2016; Cremer and Smitherman, 1980). Silver and bighead carp (*Hypophthalmichthys nobilis*) pose a significant threat to these freshwater ecosystems because they outcompete native species across the trophic hierarchy (Solomon et al., 2016). In particular, silver carp feed on a broad range of particle sizes from 4 to 85 μ m (Cremer and Smitherman, 1980; Battonyai et al., 2015; Zhou et al., 2009), making them an effective competitor for planktonic resources in the eutrophic rivers of the Mississippi River basin ecosystem (Freedman et al., 2012). Cohen

and Hernandez (2018) hypothesized that the greatly modified filtering apparatus of silver carp aids in the capture of particles so small that they are generally only consumed by invertebrates.

The gill rakers of silver carp are morphologically distinct from those of previously described chondrichthyan or bony fishes, including those of bighead carp. The filtering apparatus of silver carp is composed of two solid filtering plates that extend dorsally from the branchial arches (Fig. 1A). Early in ontogeny, individual gill rakers stitch together, creating a mesh-like plate that continues to fuse together with secondary dermal bone modifications (Cohen and Hernandez, 2018). In addition, the inner and outer faces of the filtering plates are morphologically distinct. The inner face (where particles are ultimately collected) is composed of a net-like matrix with uniformly sized mesh (~ 45 μ m wide) spanning the surface. The outer face (over which water flows) is composed of long, initially parallel channels pitted with openings of diverse sizes. These channels and associated openings are supported by layers of dermal bone and epithelium and make up three distinct regions dorsal to ventral (Cohen and Hernandez, 2018).


Gill rakers used in filter feeding show enormous morphological diversity with structures adapted to increasing efficiency of prey capture and retention. Many filter-feeding clupeiforms have elongated gill arches with rakers strongly resembling teeth on a comb (Almeida et al., 2013; Friedland, 1985). Such elongated and densely packed gill rakers along the branchial arches (Friedland, 1985) increase the efficiency of filtration in these individuals. Bighead carp also have long, but flattened, comb-like gill rakers (Fig. 1B) with secondary bony modifications (on every eighth raker) that appear early during ontogeny (Cohen and Hernandez, 2018); these rakers are similar to those seen in the filter-feeding fish *Opisthonema libertate* (Berry and Barrett, 1963) and *Brevoortia tyrannus* (Friedland, 1985). Two types of gill rakers (referred to as broad and narrow rakers) create the filter of bighead carp (Howes, 1981; Jennings, 1988; Cohen and Hernandez, 2018). Although in both bighead and silver carp two sets of modified gill rakers extend from each branchial arch, creating an acute V-shape (Cohen and Hernandez, 2018; Jirasek et al., 1981; Boulenger, 1901), the underlying anatomy of their gill rakers is quite different.

Filter-feeding fishes use a variety of mechanisms for moving water into the mouth and across filtering structures during feeding, with some fishes using ram suspension while others may be pump filter feeders (Lazzaro, 1987; Sanderson and Wassersug, 1990). During filtration, fluid enters the buccal cavity through the mouth, comes into contact with the filtering apparatus and then exits over the respiratory epithelium. Ram suspension feeders swim forward with their mouths wide open, continuously moving fluid over their filtering apparatus (Sanderson and Wassersug, 1990). Alternatively, pump filterers such as silver and bighead carp use opercular pumping in combination with hyoid depression to bring fluid into the buccal cavity and over the filtering apparatus.

In addition to filtering, the filtration apparatus (i.e. gill rakers) must also aggregate particles of food. In many ram suspension feeders, the

¹Department of Biological Sciences, The George Washington University, Science and Engineering Hall, 800 22nd St NW, Washington, DC 20052, USA. ²Department of Biological Sciences, New Jersey Institute of Technology, University Heights, Newark, NJ 07102, USA.

*Author for correspondence (phernand@gwu.edu)

 L.P.H., 0000-0001-9616-7777; B.E.F., 0000-0003-0049-965X

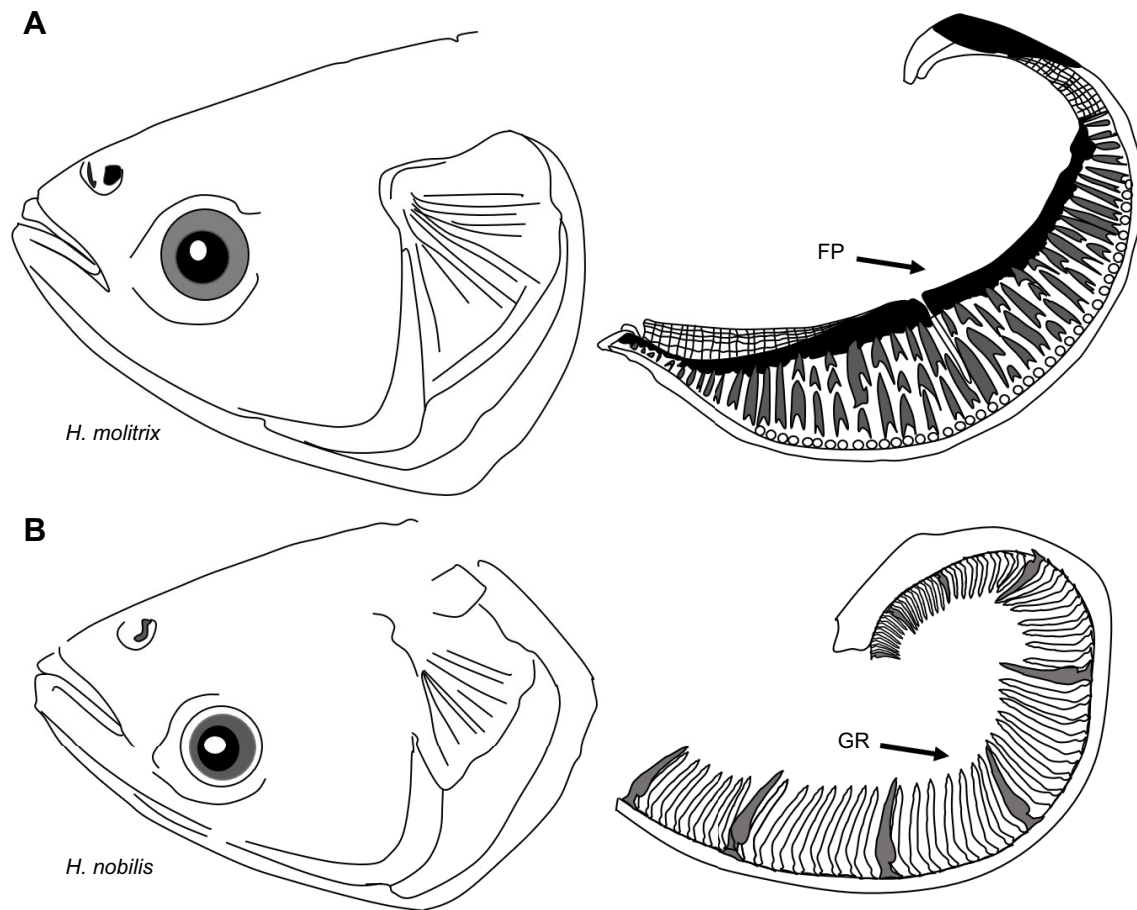


Fig. 1. Line drawing displaying the anatomical differences between the filtering anatomy in *Hypophthalmichthys molitrix* (silver carp) and *H. nobilis* (bighead carp). The filtering apparatus of silver carp (A) is composed of robust filtering plates (FP; formed by fusion of individual gill rakers), while the filtering apparatus of bighead carp (B) is composed of elongate and flat gill rakers (GR).

task of aggregation is accomplished via hydrosol or cross-flow filtration (Sanderson et al., 2001, 2016; LaBarbera, 1984; Smith and Sanderson, 2013; Paig-Tran et al., 2013). However, in several teleostean fishes, aggregation is not solely accomplished by the filtering apparatus; rather, epibranchial organs act as secondary aggregation structures enhancing bulk transport to the pharynx. Silver and bighead carp both possess large epibranchial organs into which the filtering structures terminate. Food retained by the filtration apparatus is brought into the epibranchial organs for aggregation (Bertmar et al., 1969) before being deposited onto the pharyngeal jaws for trituration and subsequent consumption.

We hypothesize that the highly modified filtering plates of silver carp are able to effectively filter out a broad range of particles using a heretofore undescribed filtering mechanism. Using volumetric particle image velocimetry (3D PIV), we visualized how the atypical anatomy of the silver carp filtering plates manipulates fluid, creating vortical flow that may ultimately serve to increase extraction efficiency. Here, we examine the 3D fluid dynamics of bighead and silver carp gill rakers under steady flow conditions.

MATERIALS AND METHODS

Sample collection and gross anatomy

Adult silver carp [*Hypophthalmichthys molitrix* (Valenciennes 1844)] and bighead carp [*Hypophthalmichthys nobilis* (J. Richardson 1845)] specimens were provided by James Lamer of

the Kibbe Field Station, Western Illinois University. All specimens arrived frozen and were then fixed in 10% buffered formalin solution. One juvenile bighead sample was provided by Chris A. Taylor and Daniel Wylie (curator and collections manager of Fishes and Crustaceans at the Prairie Research Institute, and Illinois Natural History Survey) and arrived fixed in 10% formalin solution. Gill raker sets from both bighead and silver carp were removed and prepared either for histology or for computed microtomography (μ CT) scans. For specimens that were μ CT scanned, the third arch was removed from similarly sized bighead and silver carp (Fig. 1) and the gill raker sets were trimmed at the ceratobranchials, leaving only the center portion (approximately one-third) of the arch to be scanned.

Scanning electron microscopy

Scanning electron microscopy (SEM) was used to visualize the epithelial elements of the gill rakers. Gill arches were removed from silver carp specimens [$N=2$; 840 and 860 mm standard length (SL)]. Fixed gill rakers were bisected along the length of the branchial arch to clearly visualize the inner and outer epithelial topography. Samples were fixed in a 2.5% paraformaldehyde/glutaraldehyde in 0.1 mol l⁻¹ cacodylate buffer (pH 7.4) solution. Samples were then placed in a dehydration series and left in 100% EtOH. Samples that had previously been fixed in formalin and placed in 70% EtOH were rehydrated through a stepwise procedure. Fully dehydrated specimens were then critical point dried with CO₂, sputter-coated

with gold palladium and visualized with a Leo 1430VP scanning electron microscope.

μCT scanning

X-ray computed microtomography (μCT) was used to visualize sections of fixed gill arches from a silver carp (880 mm SL) and a bighead carp (1153 mm SL). The specimens were scanned on the Bruker Skyscan 1275 located at Microphotonics Inc. (Allentown, PA, USA) at 80 kV and 125 μA with 50 ms exposure time and a 1 mm aluminum filter. Voxel size was 15.2 μm for the silver carp gill raker plate and 17.0 μm for the bighead carp gill raker set. Mimics Innovation Suite version 18 (Materialise Inc., Leuven, Belgium) was used to create digital stereolithography models of the gill structure, scaled by a factor of four (Table 1), which were then printed with a FormLabs Form1+ resin printer. A juvenile bighead carp head (140 mm SL) was scanned on a Bruker Skyscan 1275 at the New Jersey Institute of Technology (Newark, NJ, USA) with a resolution of 25 μm. Scan parameters were 80 kV, 125 μA with 46 ms exposure time and a 1 mm aluminum filter. The specimen was packaged in a sealable plastic container for scanning. Finally, a juvenile silver carp specimen (190 mm SL) was scanned at 28 μm on a Bruker Skyscan 1173 at the Karl F. Liem Imaging Center at Friday Harbor Laboratories. This specimen was used for making figures and was not part of the PIV experiments.

3D PIV

Fixed gill rakers and 3D printed models based on 15.2 μm and 17.0 μm voxel size μCT scans of adult silver and bighead carp were placed into a recirculating flow tank within the volume imaged by the volumetric imaging camera system (V3V, TSI Inc.). Each model was secured to a metal rod at the center of the flow tank. PIV data were captured ahead of the rod so as to not capture vorticity resulting from the rod interfering with flow. A single gill raker was used in this study as our primary intention was to examine the nature of surface interaction effects of particle-laden fluid with the highly modified gill raker morphology.

Our goal here was to better understand how these two very different filtering architectures interacted with fluid. This study thus represents a preliminary investigation into the actual hydrodynamics of silver carp filter feeding. Future work entails using pulsed flow as well as multiple arches so that potential edge effects from other structures can be taken into account. If we had used adjacent gill raker plates, the fluid would likely increase in velocity owing to a narrowing of this inter-gill plate space. We examined the effect of such increases in velocity by directly increasing flow speed. Although we realize that the set-up of these experiments did not replicate the exact flow regime within the buccal cavity of feeding fish, it did allow us to understand how the complex external topography of these single stiff gill raker plates would affect fluid flow. Future experiments will systematically add other aspects of this complex trophic anatomy, allowing us to obtain a more realistic view of how these fish can manipulate flow during filter feeding.

Table 1. Reynolds (*Re*) and Froude (*Fr*) numbers of bighead and silver carp gill rakers scaled to an equivalent body length of 80 cm in flow at 0.25, 0.5, 0.75 and 1.0 body lengths (BL) s⁻¹

	0.25 BLs ⁻¹	0.5 BLs ⁻¹	0.75 BLs ⁻¹	1.0 BLs ⁻¹
Flow tank speed (cm s ⁻¹)	5.0	10.0	15.0	20.0
<i>Re</i>	6 126	12,253	18,379	24,506
<i>Fr</i>	0.046	0.092	0.139	0.184

For each species, three runs each of two orientations at four different speeds [0.25, 0.5, 0.75 and 1.0 body lengths (BL) s⁻¹] were collected for fluid dynamic analysis; flow speeds were selected to match the Reynolds number of scaled-up models (Table 1). Although carp may feed using a pumping mechanism (Smith, 1989), this is only a factor if considering the flow reversal effect; instead, the focus of this project was on the filtration effect, in which water travels in the same direction during constant or pumping flow. Neutrally buoyant 50 μm particles within the volume of interest were illuminated by a 100 mJ Nd:YAG dual-head pulse laser, pulsed at a frequency of 50 Hz. The V3V camera system has three independent lenses and CCD arrays (2048×2048) that were calibrated by traversing a known target across the transverse (*Z*) plane of the flow tank, in the volume and downstream of where the models were located. Groups of image pairs (one pair per camera, three pairs total) were captured at 50 Hz with 1.2 ms between each image pair, at 12 bit resolution. The volume imaged was 14×14×12 cm, and for each image pair approximately 80,000 particles were identified in all three images, and from these approximately 40,000 triplets representing three views of the same particle were identified and tracked between laser pulses. These particles were gridded to give a final volumetric matrix of 57×57×48 vectors (=155,952 total vectors within the volume). The resulting vector files were imported into Tecplot 360 (Tecplot, Inc., Bellevue, WA, USA) to reconstruct 3D fluid structures for analysis. Vortical isosurfaces were defined using vorticity magnitude and colored by *Z*-vorticity. For statistical analysis of flow results, we used an additive linear model (in R) to describe the effect of species and flow tank speed on mean maximum vorticity magnitude. A *t*-test was used to compare mean maximum vorticity between bighead and silver carp.

RESULTS

Bighead carp

Gill raker morphology

The filtering apparatus of bighead carp was composed of a set of elongate and flat gill rakers that extended from the ceratobranchial and epibranchial and ultimately terminated in the epibranchial organ (Fig. 1B). Two sets of gill rakers attached to each branchial arch to create a V-shaped structure (Fig. 2A) with a food transport groove (where the majority of food particles were found) immediately dorsal to the ceratobranchial. The gill raker sets were not equal in height, with the lateral set of gill rakers approximately 1 cm shorter than the medial set; however, they were even in height as they entered the epibranchial organ.

Each gill raker set (the two rows of gill rakers extending from each branchial arch) was composed of fairly tightly packed and elongated, flattened gill rakers (Fig. 2A, clear and stain) that were covered in an epithelium rich in mucus-secreting goblet cells. Every eighth to ninth individual gill raker was further modified into a blade-like shape (Fig. 1B) where the edge of the blade was oriented away from the intra-gill raker space.

Volumetric PIV

The filtering model was oriented in the flow tank with the dorsal ends of the filtering sets facing at an angle towards the oncoming flow, resulting in fluid moving across the filtering plates in an anteroposterior and dorsoventral direction (Fig. 2A, blue CT reconstructions with arrow in direction of fluid flow), an angle of attack that seemed reasonable given previous work on filtering fishes. At 0.25 BL s⁻¹, the mean maximum vorticity magnitude was 0.12±0.003 s⁻¹. At 0.5 BL s⁻¹, the mean maximum vorticity was 0.19±0.007 s⁻¹. The greatest mean maximum vorticity

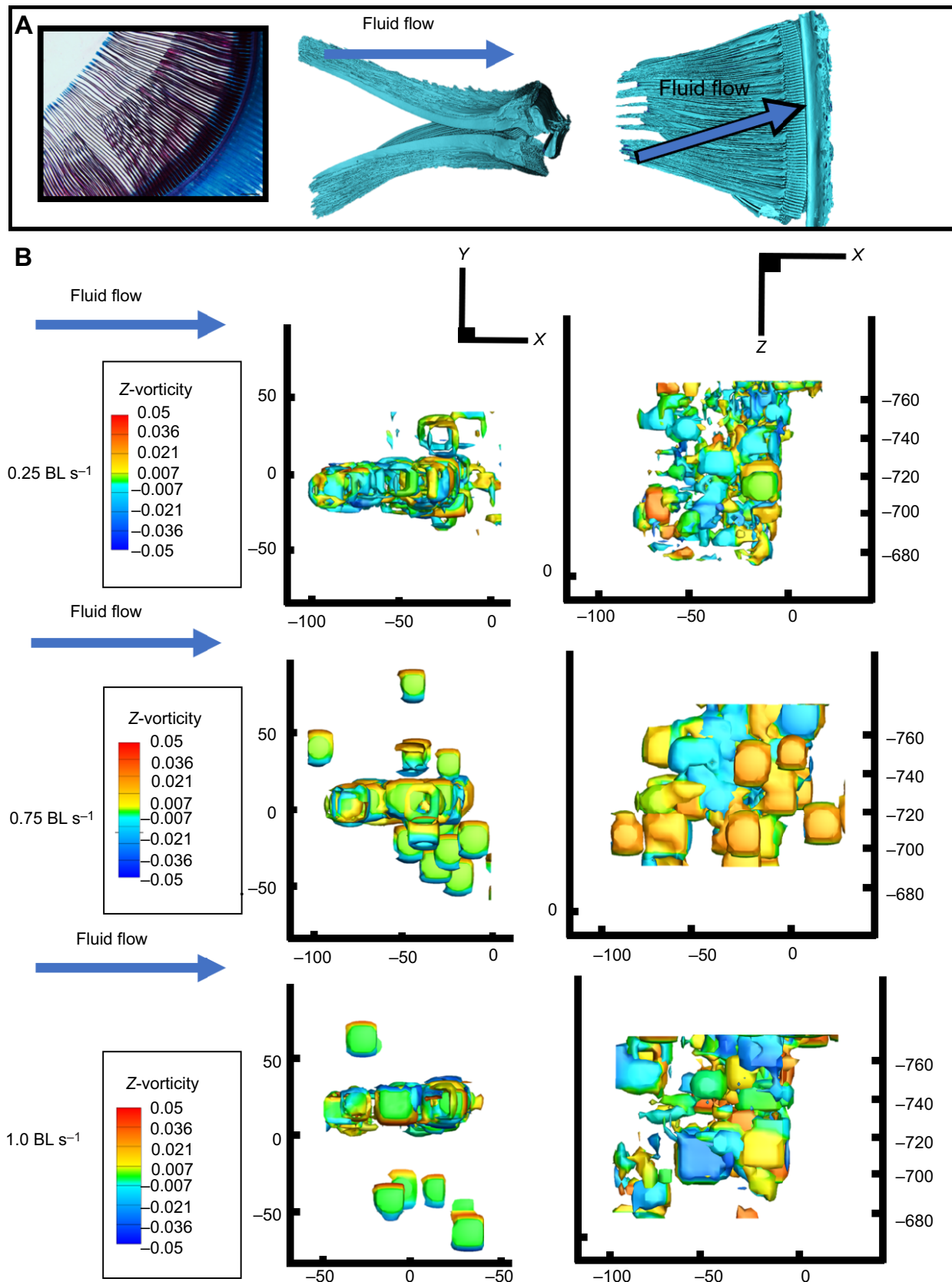


Fig. 2. Gill raker structure and particle image velocimetry (PIV) results from bighead carp. (A) Bighead carp have a filtering apparatus composed of elongate individual rakers extending from the branchial arches (left, clear and stained arch from 200 mm SL bighead carp; right, μ CT scans of 1153 mm SL bighead carp). Gills (blue) can be seen on the opposite side of the gill rakers (purple) in the clear and stained image. Gill filaments have been removed from the two CT reconstructions. (B) PIV indicated that at all tested speeds, the bony modifications of the bighead gill raker set created turbulence as fluid moved across the structure. Vortices rolled away and were rebounded from the filtering apparatus. The axes are dimensions in mm.

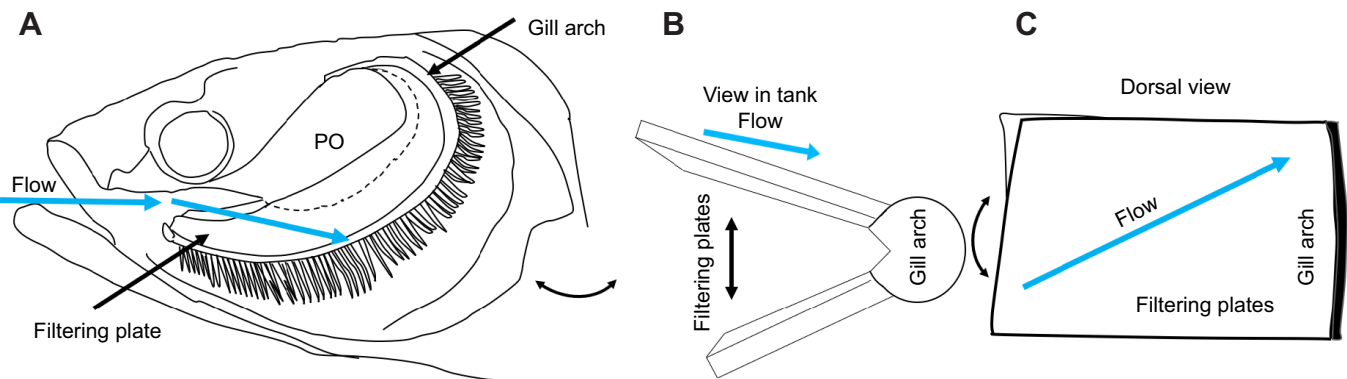


Fig. 3. Direction of flow over filtering plates in silver carp. (A) Schematic illustrating how silver carp gill raker plates were situated with respect to flow. PO, palatal organ. (B) Flow moved across the filtering models in the anterior to posterior direction from the dorsal edge of the model to the ventral base. (C) Direction of fluid flow over the filtering plate from a dorsal perspective.

magnitude ($0.297 \pm 0.013 \text{ s}^{-1}$) occurred at a flow velocity of 0.75 BL s^{-1} ; when flow velocity was increased to 1.0 BL s^{-1} , the mean maximum vorticity magnitude decreased slightly to $0.279 \pm 0.013 \text{ s}^{-1}$. All bighead carp experimental data sets were isosurfaced at a threshold of 0.035 s^{-1} to produce the most-complete vortical ring structures.

At 0.25 BL s^{-1} , the slowest speed in our data set, there was almost no development of vortical structure across the model; instead, only partial vortices were formed. These vortices were slow moving and characterized by the haphazard motion of particles away from the filtering model (Fig. 2B, first row). Flow appeared largely disorganized and was not obviously impacted by the morphology of the filter. At 0.75 BL s^{-1} we observed the development of vortices traveling lengthwise along the gill raker model from the anterior to the posterior end of the ceratobranchial (Fig. 2B, second row). Similar to data collected at 0.25 BL s^{-1} , at 0.5 and 0.75 BL s^{-1} , vortices did not exhibit an organized flow pattern; instead, particles moved away from the filter if their trajectory did not permit them to pass opportunistically between

gill rakers (Fig. 2B, second row). Finally, at 1.0 BL s^{-1} , fluid was moving too quickly to be meaningfully impacted by the filtering apparatus, again showing no development of strong vortical flow (Fig. 2B, third row).

Silver carp

Gill raker morphology

The filtering anatomy of silver carp was composed of paired gill raker plates extending from each branchial arch (Figs 3, 4A,B), except for the fifth branchial arch (the arch supporting the pharyngeal teeth), which contained only one filtering plate. Each set of filtering plates created a distinctive V-shape as they connected to the branchial arches (Fig. 4B). Each individual plate was formed from a row of gill rakers that stitched together and was overgrown by additional dermal bone. These paired plates had morphologically distinct faces, with the inner face composed of a net-like matrix and the outer face being more topographically complex. The more complex side (Fig. 4C) was the side that experienced water flow.

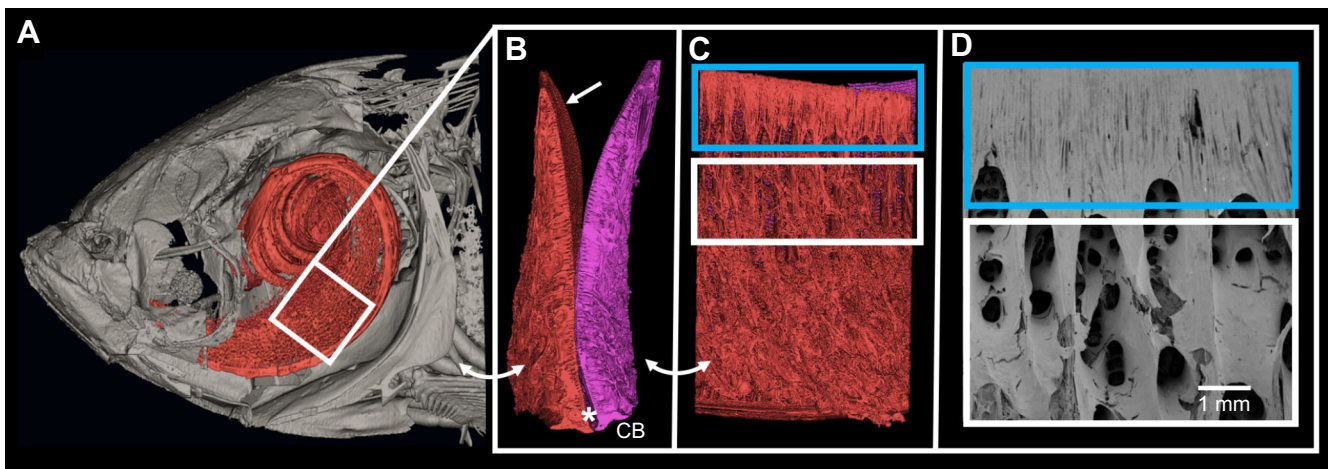


Fig. 4. Anatomy of the filtering plates in silver carp. (A) CT scan of juvenile silver carp (100 mm SL; there is no significant change in the morphology of the filtering plates from 100 to 900 mm SL). The gill raker plates (in red) extend from the most anterior portion of the buccal cavity and curve upwards as they approach the pharynx, seen here in a lateral view. White box highlights region along the arch where the filtering plate model was scanned from an adult specimen. (B) CT scan of adult (860 mm SL) silver carp filtering plates. Two filtering plates attach to a food transport groove (asterisk) dorsal to the ceratobranchial (CB) and form an acute V-shape, seen here in cross-section. Straight arrow points to the inner morphology of the filtering plate that is composed of a net-like matrix. This is in contrast to C, which highlights the outer topography over which fluid flows. (C,D) CT and SEM (respectively) of adult filtering plate (860 mm SL) showing the outer epithelial topography. The outer topography can be separated into three morphologically distinct regions. Region 1, fused dorsal tips (blue box); region 2, significant increase in topography created by parallel channels and openings of different sizes (white box); region 3 (the remaining plate), channels oriented at an angle to the incoming streamline of flow.

Characterized by long parallel channels pitted with round openings of different sizes, the outer face of the filtering plate was divided into three discrete regions. The first region (Fig. 4C,D, blue box) was made up of tightly fused dorsal tips of individual gill rakers which formed a solid and flat leading edge of the filtering plate. The second region (Fig. 4C,D, blue box) included a significantly more topographically complex series of parallel channels pitted with holes ranging in size from 20 to 85 μm in diameter (Fig. 4C,D, white box). Importantly, there was a steep change in depth between the first region (made up of fused dorsal tips) and the second region (characterized by pitted channels) that may be hydrodynamically relevant during feeding. Finally, the third region of the filtering plate was located two-thirds of the way from the dorsal extreme of the plate (the unboxed region of Fig. 4C). This final region was still composed of channels, but they were slightly curved channels. Water entered the buccal cavity through the mouth moving antero-posteriorly as well as dorsoventrally over the

filtering apparatus (Fig. 3). The epithelium that covered the filtering plates was filled with an abundance of mucus-producing goblet cells.

Volumetric PIV

The mean magnitude of vortices interacting with gill raker plates of silver carp was a full order of magnitude larger than that seen in bighead carp ($P=1.26\times 10^{-13}$). We found significant main effects of species ($P=0.001$) and flow tank speed ($P<0.05$) in an additive linear model of species and flow tank speed on mean maximum vorticity. All silver carp experimental data sets were isosurfaced at a threshold of 0.35 s^{-1} to produce the most-complete vortical ring structures. At 0.25 BL s^{-1} , the mean maximum vorticity magnitude was $1.23\pm 0.09\text{ s}^{-1}$. Vortices began to develop at the interface of regions 2 and 3, where the channels containing different-sized openings changed in orientation along the filtering plate (Fig. 5). Initially, vortices developed in the direction of flow; however, they

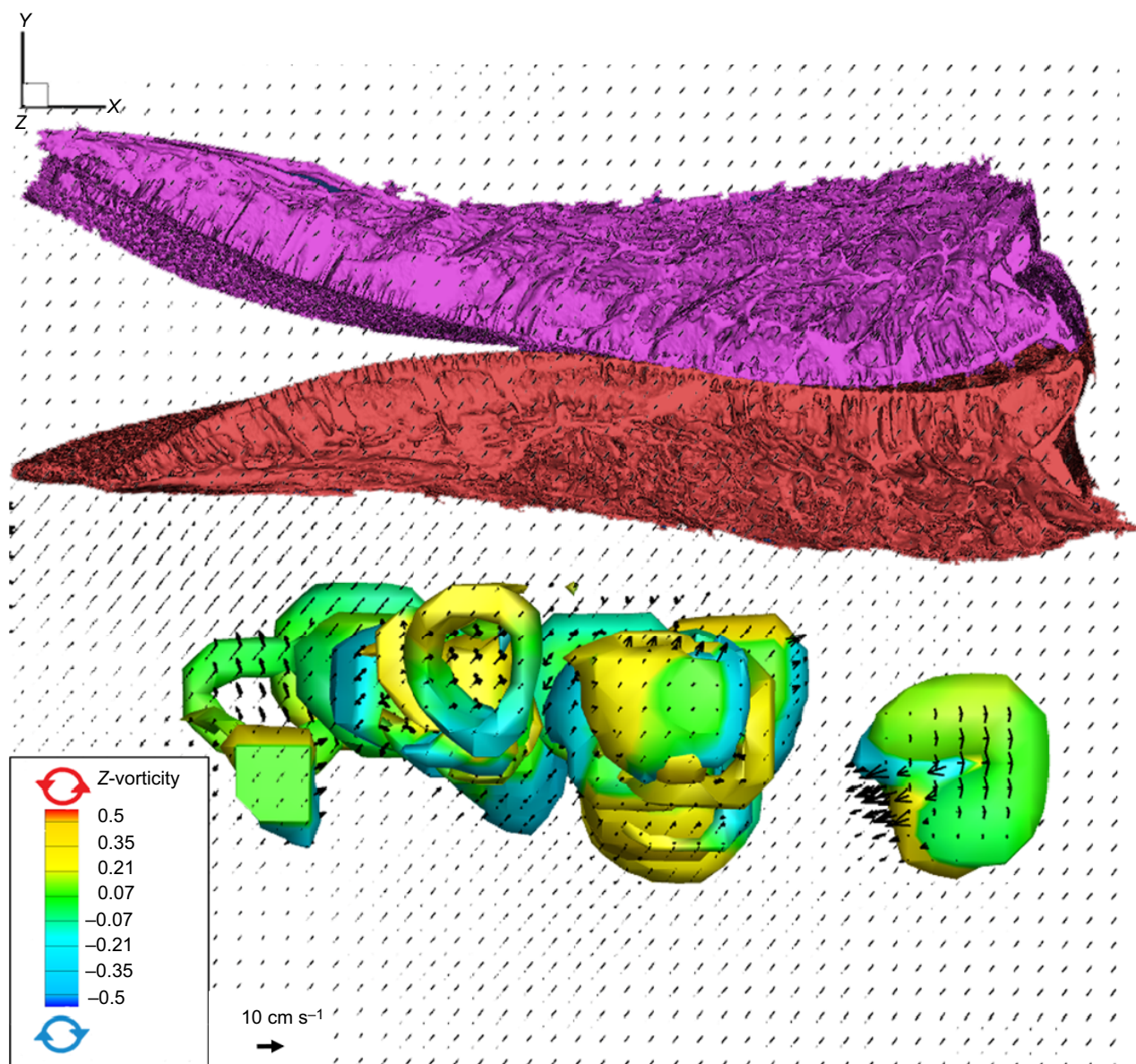


Fig. 5. Particle volumetric data from a flow speed of 0.25 BLs^{-1} . Three-dimensional capture of vortices moving across the filtering model at the slowest speed of 0.25 BLs^{-1} . Lateral view of model, isosurface value of 0.35 s^{-1} . Vortices were slow moving and flow became disorganized as particles came into contact with region 3 of the filtering plates.

were slow moving, and as fluid came in contact with the third region of the filtering plate the flow became disorganized (Fig. 5). Vortices did not lose momentum along the filtering model, as indicated by rings of the same proportional size and color, and maintained interaction with the filtering plate instead of being shed as was seen with the bighead model.

Beginning at 0.5 BL s^{-1} , the mean maximum vorticity magnitude increased to $1.37 \pm 0.09 \text{ s}^{-1}$. At this speed, vortical flow developed primarily along the second region of the filtering plate. Some of the vortices began to change in direction at the interface of region 2 and 3, rotating perpendicular to the free-stream flow, albeit at a relatively low vorticity (Fig. 6).

Peak vortical flow at the speeds tested occurred at 0.75 BL s^{-1} ; at this speed, the mean maximum vorticity magnitude was $1.46 \pm 0.12 \text{ s}^{-1}$, the highest for any speed from either species. Vortical flow was first initiated at the interface of regions 1 and 2, where the morphology of the filter changes from a relatively flat surface (where the dorsal tips are fused) to porous channels with pronounced topography (Fig. 7). Fluid moved quickly from region 1

to region 2 and changed from laminar to vortical flow. This transition was characterized by the development of large, fast-moving vortices seen at the upstream end of the model. Vortical flow continued to develop through region 2 in the dorsoventral and anteroposterior direction and did not decelerate as a result of shearing forces; rather, we saw that vorticity was maintained throughout the length of the model. At the interface of regions 1 and 2 of the filtering plate, roughly two-thirds of the way downstream on the plate, the vortices turned nearly 90° (Fig. 7, box). This change in vortical flow was concurrent with a change in the direction of the channels between regions 2 and 3.

At 1.0 BL s^{-1} , the mean maximum vorticity magnitude was $1.21 \pm 0.06 \text{ s}^{-1}$. Vortices were aggregated towards the downstream half of the filtering apparatus, with some vortices being well developed and spinning towards channels (Fig. 8). Moreover, some vortices changed in direction concomitant with a change in the aforementioned underlying anatomy.

Overall, 0.75 BL s^{-1} appeared to be the optimal speed for both development and organization of strong vortical flow (Fig. 9). At

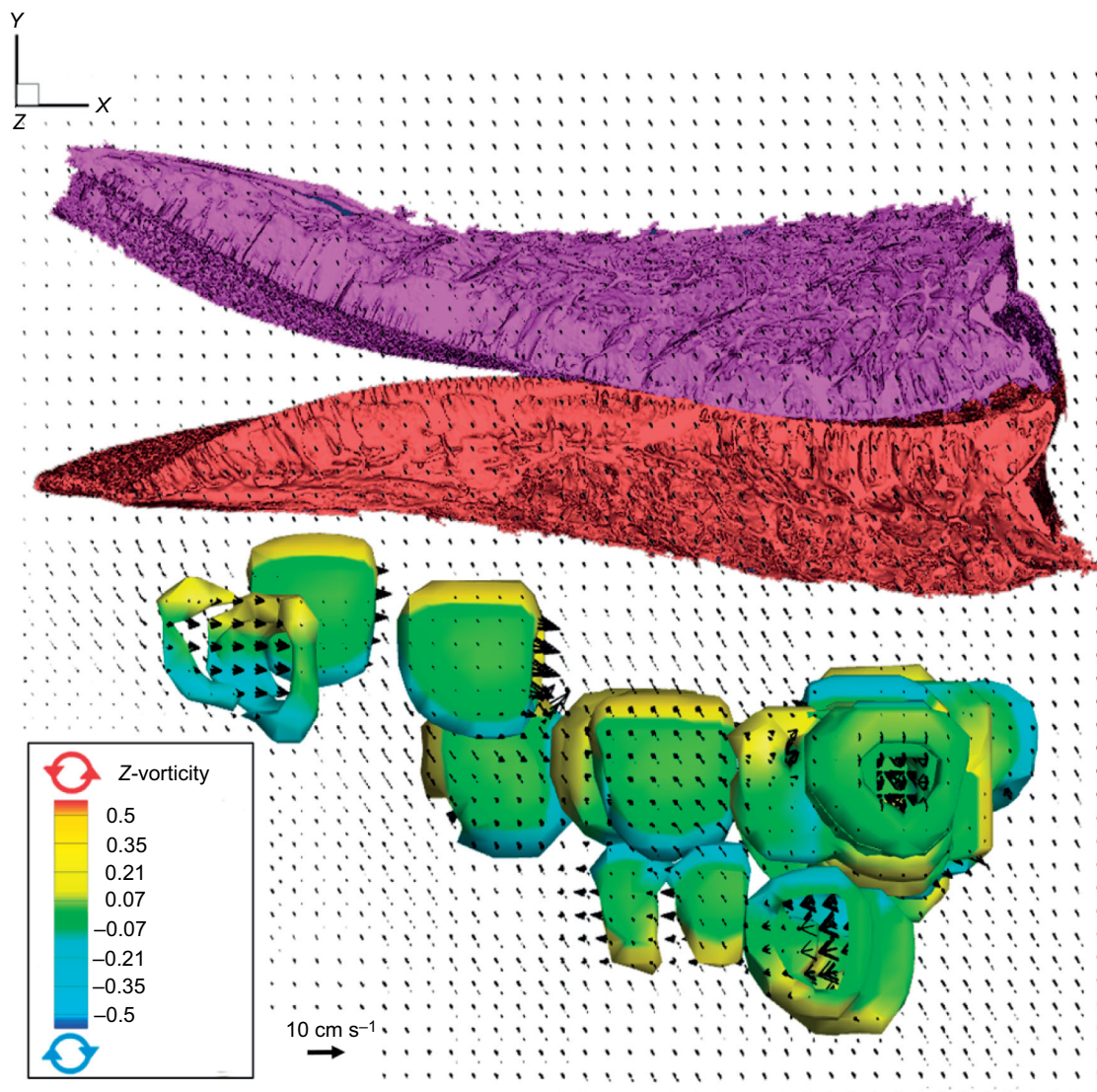


Fig. 6. Particle volumetric data from a flow speed of 0.5 BL s^{-1} . Lateral view of model showing three-dimensional snapshot of fluid interaction with the filtering model isosurfaced at 0.35 s^{-1} . Increased flow speed was correlated with an increase in vortices; however, these vortices were slow moving, and as fluid interacted with region 3, flow became disorganized and vortices were shed away from the model.

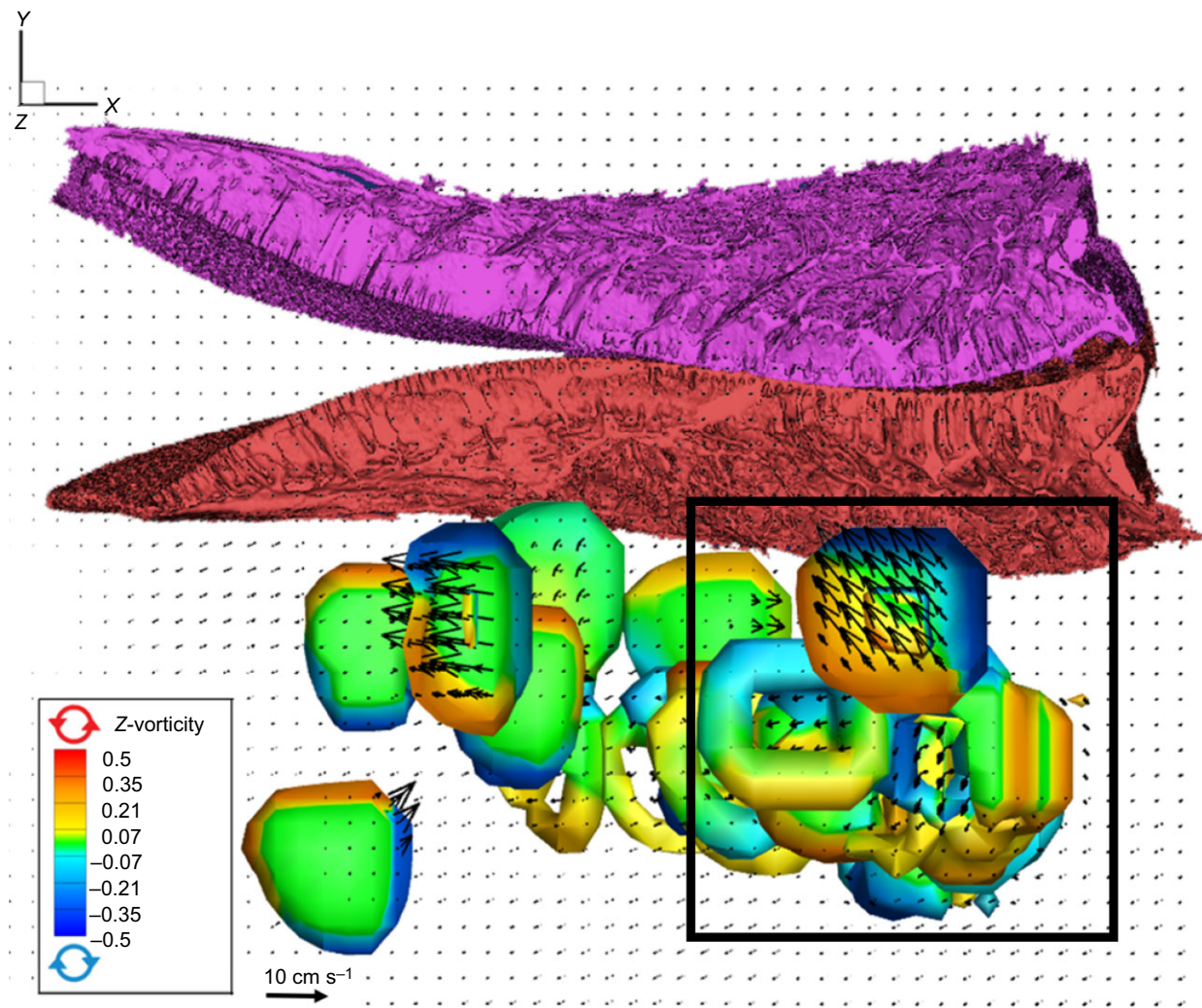


Fig. 7. Particle volumetric data from a flow speed of 0.75 BL s^{-1} . Strong vortical flow developed at the transition from region 1 (flat surface composed of fused gill rakers) to region 2, where the topography of the filter increased. This vortical flow was developed and maintained along the entirety of the model and did not decelerate, as indicated by vortices of the same proportion. At the interface of regions 2 and 3, we saw a stark directional change in the vortices (box), with vortical flow in the direction of the epibranchial organ. This directional change was concomitant with a change in the underlying anatomy, where the channels were oriented at an angle with respect to the incoming flow.

this speed, flow was tightly correlated with the underlying structure of the channels within the filtering model. As fluid moved across the flat, smooth region 1 and moved into the channels of region 2, it established a vortical flow that was laterally constrained by the walls of the channels. These vortices maintained vorticity magnitude while traveling through the channels and did not appear to decelerate as a result of shearing forces. The results indicated a significant effect of free-stream fluid speed on vortical flow production and fluid–structure interactions ($P < 0.001$). The variance in maximum vorticity between bighead and silver carp was 0.01 and 0.42, respectively.

DISCUSSION

Silver and bighead carp are filter feeders that consume a wide range of phytoplankton and zooplankton (Cremer and Smitherman, 1980; Smith, 1989; Solomon et al., 2016; Sampson et al., 2009), and both species have had a detrimental effect on overall community structure in the upper Mississippi River basin (Solomon et al., 2016; Zhang et al., 2016). Even though silver and bighead carp are closely related and effective filter feeders, their filtering apparatuses are morphologically distinct.

The filtering apparatus of silver carp is characterized by rigid filtering plates formed from individual gill rakers stitching together during early ontogeny (Cohen and Hernandez, 2018). The outer, topographically complex face of the filter can be separated into three fairly discrete regions: the first and most dorsal region is relatively flat and composed of fused gill raker tips; the second region is composed of parallel rows of channels filled with pores of different sizes; the third and final region is composed of channels that are oriented at an angle to the parallel rows. The stitching together of individual gill rakers (to form a solid plate as seen in silver carp) has not been previously described in any other teleostean fish.

In contrast, the filtering apparatus of bighead carp is more reminiscent of many other teleostean filter feeders as exemplified by *Brevoortia*, *Anchoa* and *Sardinella* (Almeida et al., 2013; Friedland, 1985). Two sets of elongated gill rakers extend from the branchial arches creating a V-shape. Moreover, every eighth individual raker is further modified with dermal bone into a blade-like shape that points away from intra-gill raker space. Importantly, the anatomy of the filtration apparatus of teleostean filter feeders often corresponds to both diet and type of filtration mechanism

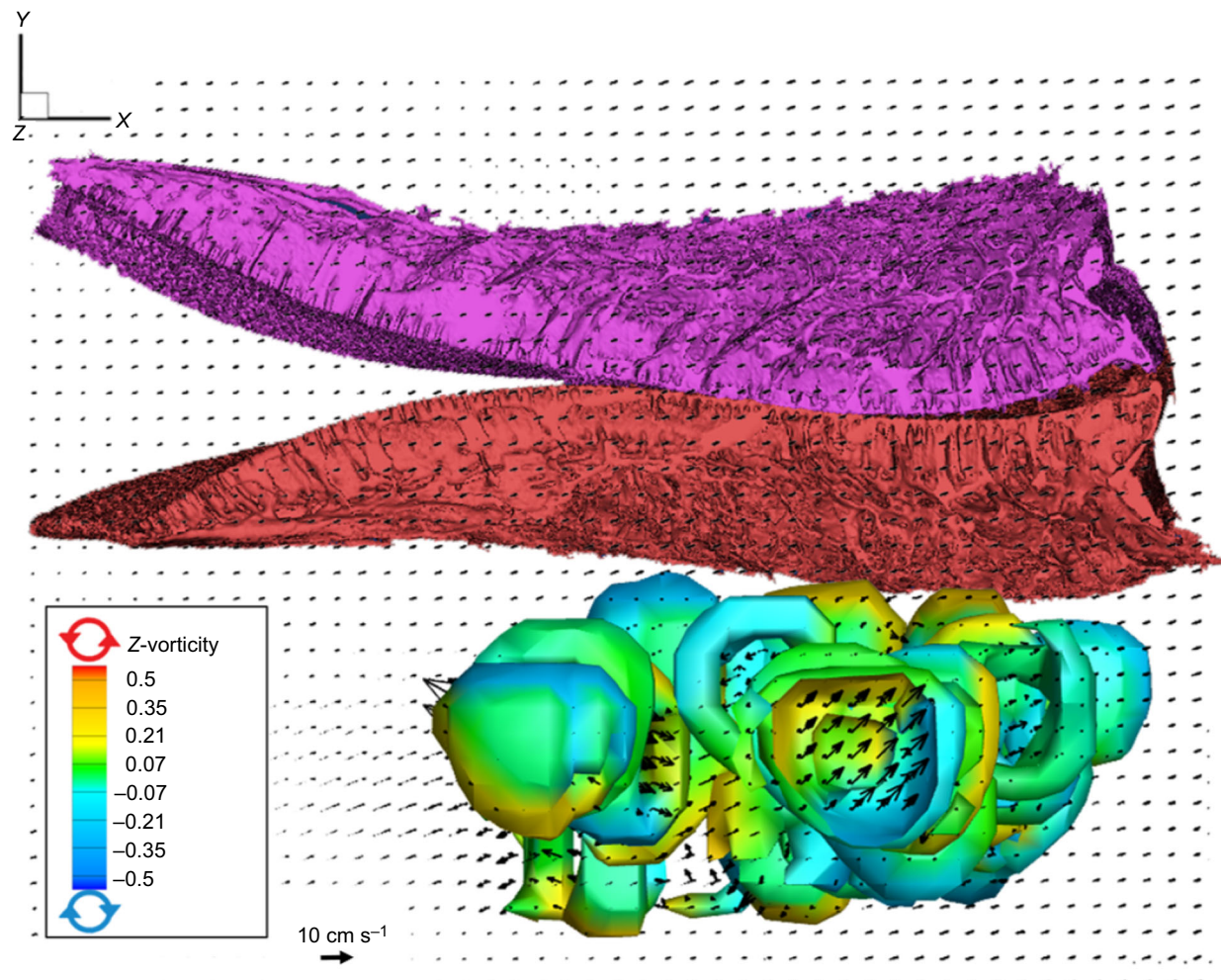


Fig. 8. Particle volumetric data from a flow speed of 1.0 BL s^{-1} . Data set from the fastest speed, isosurfaced at 0.35 s^{-1} , lateral view. Vortices were aggregated towards the back half of the model. At this speed, fluid was moving too quickly across the model for flow to be entrained by the filtering model.

(Almeida et al., 2013; Friedland, 1985). Unfortunately, little experimental data exist describing the type of filtration used in many filter feeders.

Our data suggest that bighead carp use a haphazard cross-flow filtration, as was apparent by vortices indicating particles tumbling away from the filtering model. During cross-flow filtration, particles of food are tangentially sheared from the incoming streamline of flow (Sanderson et al., 2001, 2016; Bott et al., 2000; Sibanda et al., 2001) resulting in said particles being aggregated at the posterior end of the pharynx (Sanderson et al., 2001; Bott et al., 2000; Sibanda et al., 2001; Smith and Sanderson, 2013). In the bighead model, as fluid interacted with the filter, particles rebounded away from the filtering model as described for some other filter-feeding teleosts (Fig. 10A,B). As bighead carp possess modified gill rakers similar to those of several other teleostean filter feeders, it is not unreasonable to extrapolate from our results to explain how other pump filter-feeding fishes may manipulate flow. Alternatively, the novel filtering anatomy of silver carp presents an opportunity to study a potentially novel or specialized filtration mechanism.

Results from this study suggest that the outer morphology of the filtering plates in silver carp initiated strong, organized vortical flow and that this organization was best developed and maintained at 0.75 BL s^{-1} ; at the slower and faster speeds tested here, strong vortical flow was neither developed nor maintained (Fig. 9). We

suspect that at slower speeds (0.25 BL s^{-1}), the change in depth from the first region of the model to the second region does not create a strong enough pressure change to induce strong vortical flow. Brooks et al. (2018) recently showed that pressure drops created across the filtering apparatus in suspension-feeding fishes are crucial to the development of vortical structures. As a result of the decrease in pressure, vortices that develop across region 2 are slow moving and do not accelerate across the model. As flow speed increased to 0.5 BL s^{-1} , there was an increase in the number and strength of vortices generated at the shelf break between regions 1 and 2. Additionally, some vortices underwent a directional change concomitant with the underlying anatomy of region 3. At slower free-stream speeds such as 0.25 and 0.5 BL s^{-1} , vortical flow decelerates as it moves downstream along the filtering model. Conversely, at faster speeds (1.0 BL s^{-1}), fluid is moving too quickly to be entrained by the underlying morphology of the filter, resulting in fluid shearing quickly past regions 1 and 2 without building organized vortical flow. As fluid encounters the third region of the filtering plate, vortices aggregate and rebound before reaching the posterior region of the filtering plate.

Only at 0.75 BL s^{-1} did we find that vortical flow was tightly organized and highly correlated with the underlying morphology of the filtering plate (Fig. 9). Upstream, fluid initially crossed the fused dorsal gill raker tips, which create a relatively flat leading edge of the

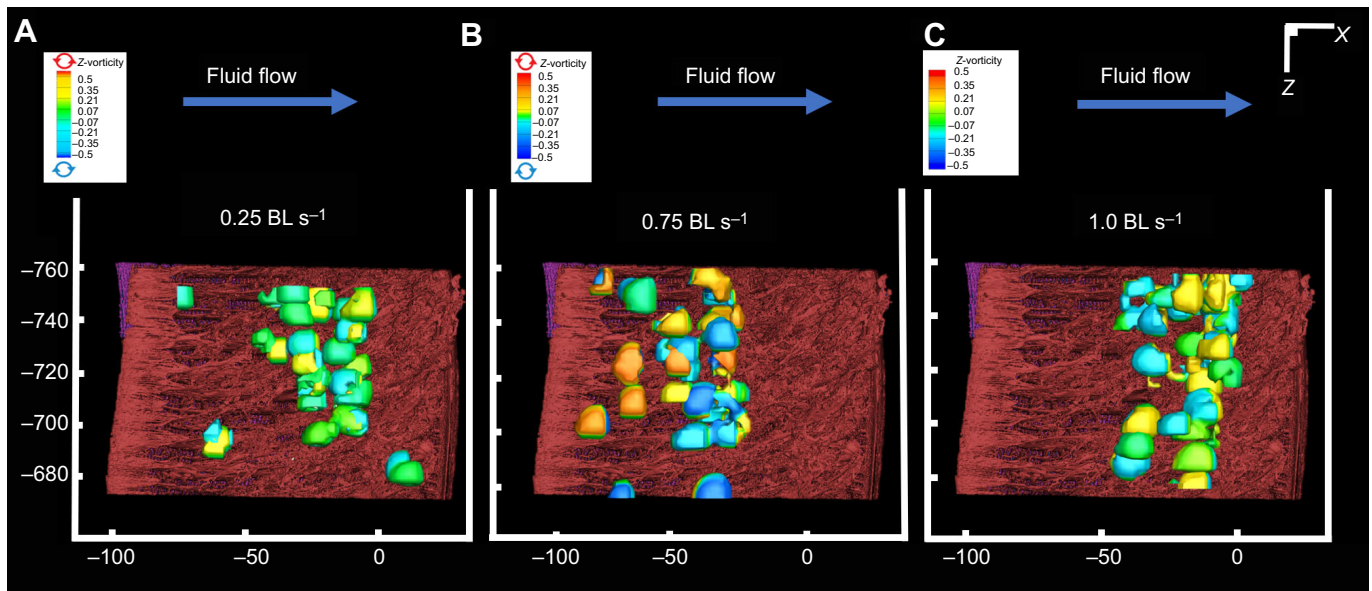


Fig. 9. Comparison of PIV data across different speeds in silver carp, from a dorsal perspective. (A) At slower speeds, the pressure drop between regions 1 and 2 did not induce strong vortical flow. As a result, vortices did not develop or become as robust across region 2, and flow became disorganized as it changed direction concomitant with a change in the underlying anatomy. (B) At 0.75 BL s^{-1} , strong vortical flow was developed and maintained across the entirety of the filter even as there was a stark directional change at the interface between regions 2 and 3. (C) At faster speeds, flow was moving too quickly to be entrained and organized by the underlying anatomy. The topography of the filtering plates instead acted as an obstruction to flow, and as a result, flow rebounded away from the filter. Axes are Z- and X-dimensions in mm.

model. At this point on the filtering plate (region 1), flow is laminar; however, as fluid moves from region 1 to region 2, there is a change in depth of the filtering model where the flat shelf ends abruptly above the deeper channels (Fig. 10E). It is at this interface between region 1 and 2 that we see the development of strong vortical flow as a consequence of fluid moving across a relatively flat surface and falling into a trough that is larger in constrained volume and more topographically complex. Vortical flow developed as fluid rolled from the shelf break and into these channels, where the narrow

channel walls may act in constraining and thus increasing the velocity of the fluid, forming forced vortices.

Forced vortices occur at low to moderate Reynolds numbers and require a continuous external source of kinetic energy to continue moving (Brooks et al., 2018), such as would be provided by buccal pumping (or continuous flow as seen within these flow tank experiments). We hypothesize (Fig. 10) that the channels on the outer face of the filtering plates constrain the fluid and produce a decrease in pressure within the channels, thereby increasing the

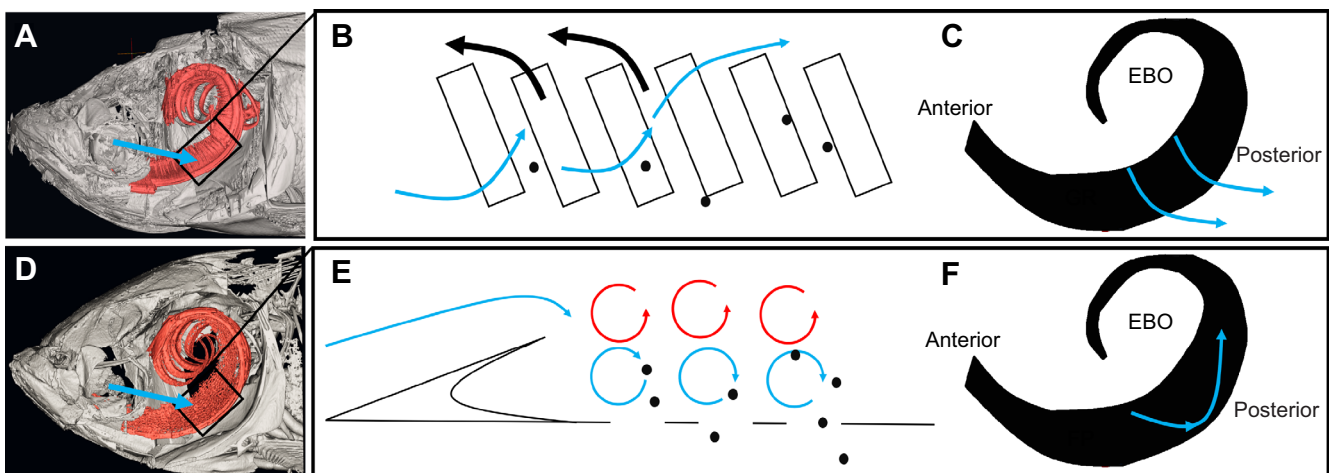


Fig. 10. Functional hypotheses for the filtration mechanisms in bighead and silver carp. (A) CT scan of bighead carp showing the filtering apparatus showing direction of fluid flow (blue arrow). (B) Proposed filtration mechanism of bighead carp. PIV indicated that fluid was haphazardly rebounded away from the filter. As fluid moved across the filtering apparatus, it entered through the individual rakers and either released particles into the intragill raker space, or particles were rebounded away from the filter (C). GR, gill rakers; EBO, epibranchial organ. (D) CT scan of silver carp showing direction of fluid flow (blue arrow). (E) Strong vortical flow was initiated at the transition between region 1 and 2 where there was a significant change in the topography of the filtering plates. Vortices continued to accelerate across the filtration plates. We hypothesize that during moments of deceleration particles may be released from the streamline of flow and pass through the many openings on the inner face of the filtering plates. (F) Moreover, as flow interacts with region 3 of the filtering plates (FP), there was a pronounced directional change in vortical structure towards the epibranchial organ (EBO).

velocity of flow. As vortices interact with the bottom surface of the channels, they are subject to deceleration as a result of friction and shearing forces. We hypothesize that during such shearing, the velocity-reduced particles of food may be released from the vortical flow and drop into the different pores found within the channels (Fig. 10E). Pores within these channels lead to the inner face of the filtering plate, where accumulated particles can be seen before they are transported to the epibranchial organ. Finally, at the interface of region 2 and 3 we find a stark directional change in the vortical flow concomitant with a change in the underlying anatomy. Importantly, this directional change is in the direction of food transport, towards the epibranchial organ (Fig. 10F). Although there are no direct measurements of swim speed during filter feeding in silver carp, it has been shown that in menhaden the smallest particles are captured at speeds just under 1.0 BL s^{-1} (Friedland et al., 1984); therefore, we rationalize that 0.75 BL s^{-1} is within the realm of probable speeds used during this type of filter feeding.

The epibranchial organ is a secondary food-aggregating organ that takes particles captured by the filtering apparatus and aggregates said particles into a bolus for transport to the esophagus (Bertmar et al., 1969; Nelson, 1967). The filtering plates of silver carp and the gill raker sets of bighead carp terminate into epibranchial organs. Additionally, small particles of food are consistently found along the food transport groove (where the two filtering plates/gill raker sets attach in a V-shape to the branchial arches) and inside the epibranchial organ, supporting the hypothesis that food captured by the filtering plates is somehow transported dorsally into the epibranchial organs. We hypothesize that the directional change in flow observed at the interface of regions 2 and 3 of the silver carp filtration model aids in the movement of particles along the filtering plates dorsally towards the epibranchial organ. This could potentially increase filtration efficiency by increasing bulk transport of particles to the pharynx.

The results presented herein suggest that the filtering plates of silver carp directly manipulate fluid to maximize particle transport, while the morphology of the filtering gill raker sets in bighead carp results in haphazard cross-flow filtration (Fig. 10). Silver carp consume a greater diversity of particle sizes than bighead carp (Smith, 1989; Battonyai et al., 2015; Cremer and Smitherman, 1980), including particles as small as $4 \mu\text{m}$. Moreover, the absolute vorticity magnitude for silver carp was an entire order of magnitude greater (0.35 to 0.035 , respectively) and peak vorticity five times greater (1.5 to 0.3 , respectively) than that in bighead carp, indicating that the silver carp filtering apparatus creates much greater vortical flow than that observed in the less modified gill raker anatomy of bighead carp. Despite having lower vorticity than silver carp, the most organized vortical flow in bighead carp was also at 0.75 BL s^{-1} , suggesting that this speed may be an optimal speed for efficient filtering in Asian carp in general. Current literature suggests that the differences seen in the bighead and silver carp filtration mechanisms do not account for the difference in diet composition or filtration efficiency (Battonyai et al., 2015). However, our results suggest that the direct manipulation of flow by the filtering plates in silver carp may increase filtration efficiency through the development of strong, organized vortical flow. Such organized flow would be essential to effectively feed on very small particles, a task readily accomplished by silver carp.

Acknowledgements

Special thanks to James Lamer at the Kibbe Field Station, John Chick of National Great Rivers Research and Education Center, Chris A. Taylor and Daniel Wylie (curator and collections manager of Fishes and Crustaceans at the Prairie Research Institute and Illinois Natural History Survey) for samples of bighead and silver carp.

Adam Summers provided CT scans of juvenile silver carp (using a Bruker Skyscan 1173 at the Karel F. Liem Bio-Imaging Center at Friday Harbor Laboratories). Additional CT scans were performed at the New Jersey Institute of Technology (Skyscan 1275). Dan Troolin (TSI, Inc.) provided flow imaging support.

Competing interests

The authors declare no competing or financial interests.

Author contributions

Conceptualization: K.E.C., L.P.H.; Methodology: K.E.C., L.P.H., C.H.C., B.E.F.; Software: B.E.F.; Validation: L.P.H.; Formal analysis: K.E.C., B.E.F.; Investigation: K.E.C., C.H.C., B.E.F.; Resources: B.E.F.; Data curation: K.E.C.; Writing - original draft: K.E.C.; Writing - review & editing: K.E.C., L.P.H., C.H.C., B.E.F.; Visualization: K.E.C., L.P.H.; Supervision: L.P.H.; Project administration: L.P.H.; Funding acquisition: L.P.H.

Funding

This work was supported by the National Science Foundation (IOS 1025845 to L.P.H.), and Harlan Award to K.E.C. from The George Washington University.

References

- Almeida, A. P. G., Behr, E. R. and Baldissarroto, B. (2013). Gill rakers in six teleost species: influence of feeding habit and body size. *Ciencia Rural* **43**, 2208-2214.
- Battonyai, I., Specziár, A., Vítál, Z., Mozsár, A., Görgényi, J., Borics, G., Tóth, L. G. and Boros, G. (2015). Relationship between gill raker morphology and feeding habits of hybrid bigheaded carps (*Hypophthalmichthys* spp.). *Knowledge Manag. Aquat. Ecosyst.* **416**, 36.
- Berry, F. H. and Barrett, I. (1963). Gill raker analysis and speciation in the thread herring genus *Opisthonema*. *Int. Am. Trop. Tuna Comm.* **7**, 113-181.
- Bertmar, G., Kapoor, B. and Miller, R. V. (1969). Epibranchial organs in lower teleostean fishes—an example of structural adaptation. *Int. Rev. Gen. Exp. Zool.* **4**, 1-48.
- Bott, R., Langeloh, T. H. and Ehreld, E. (2000). Dynamic cross flow filtration. *Chem. Eng. J.* **80**, 245-249.
- Boulenger, G. A. (1901). XXV. On the presence of a superbranchial organ in the cyprinoid fish *Hypophthalmichthys*. *Ann. Mag. Nat. Hist. Ser.* **8**, 186-188.
- Brooks, H., Haines, G. E., Lin, M. C. and Sanderson, S. L. (2018). Physical modeling of vortical cross-step flow in the American paddlefish, *Polyodon spathula*. *PLoS ONE* **13**, e0193874.
- Cohen, K. E. and Hernandez, L. P. (2018). Making a master filterer: ontogeny of specialized filtering plates in silver carp (*Hypophthalmichthys molitrix*). *J. Morphol.* **279**, 925-935.
- Cremer, M. C. and Smitherman, R. O. (1980). Food habits and growth of silver and bighead carp in cages and ponds. *Aquaculture* **20**, 57-64.
- Freedman, J. A., Butler, S. E. and Wahl, D. H. (2012). *Impacts of Invasive Asian Carps on Native Food Webs (Final Report)*. Urbana-Champaign, IL: University of Illinois, Kaskaskia Biological Station.
- Friedland, K. D. (1985). Functional morphology of the branchial basket structures associated with feeding in the Atlantic menhaden, *Brevoortia tyrannus* (Pisces: Clupeidae). *Copeia* **1985**, 1018-1027.
- Friedland, K. D., Haas, L. W. and Merriner, J. V. (1984). Filtering rates of the juvenile Atlantic menhaden *Brevoortia tyrannus* (Pisces: Clupeidae), with consideration of the effects of detritus and swimming speed. *Mar. Biol.* **84**, 109-117.
- Howes, G. (1981). Anatomy and phylogeny of the Chinese major carps *Ctenopharyngodon* Steind., 1866 and *Hypophthalmichthys*, 1860. *Bull. Br. Mus. Nat. Hist.* **41**, 1-52.
- Jennings, D. P. (1988). *Bighead Carp (Hypophthalmichthys nobilis): A Biological Synopsis*. Biological Report 88. US Fish and Wildlife Service.
- Jirasek, J., Hampl, A. and Sirotek, D. (1981). Growth morphology of the filtering apparatus of silver carp (*Hypophthalmichthys molitrix*). *Aquaculture* **26**, 41-48.
- LaBarbera, M. (1984). Feeding currents and particle capture mechanisms in suspension feeding animals. *Am. Zool.* **24**, 71-84.
- Lazzaro, X. (1987). A review of planktivorous fishes: their evolution, feeding behaviours, selectivities, and impacts. *Hydrobiologia* **146**, 97-146.
- Nelson, G. J. (1967). Epibranchial organs in lower teleostean fishes. *J. Zool.* **153**, 71-89.
- Paig-Tran, E. M., Kleinteich, T. and Summers, A. P. (2013). The filter pads and filtration mechanisms of the devil rays: variation at macro and microscopic scales. *J. Morphol.* **274**, 1026-1043.
- Sampson, S. J., Chick, J. H. and Pegg, M. A. (2009). Diet overlap among two Asian carp and three native fishes in backwater lakes on the Illinois and Mississippi Rivers. *Biol. Invasions* **11**, 483-496.
- Sanderson, S. L. and Wassersug, R. (1990). Suspension-feeding vertebrates. *Sci. Am.* **262**, 96-101.

- Sanderson, S. L., Cheer, A. Y., Goodrich, J. S., Graziano, J. D. and Callan, W. T.** (2001). Crossflow filtration in suspension-feeding fishes. *Nature* **412**, 439-441.
- Sanderson, S. L., Roberts, E., Lineburg, J. and Brooks, H.** (2016). Fish mouths as engineering structures for vortical cross-step filtration. *Nat. Commun.* **7**, 11092.
- Sibanda, V., Greenwood, R. W. and Seville, J. P. K.** (2001). Particle separation from gases using cross-flow filtration. *Powder Technol.* **118**, 193-202.
- Smith, D. W.** (1989). The feeding selectivity of silver carp, *Hypophthalmichthys molitrix*. *J. Fish Biol.* **34**, 819-828.
- Smith, J. C. and Sanderson, S. L.** (2013). Particle retention in suspension-feeding fish after removal of filtration structures. *Zoology* **116**, 348-355.
- Solomon, L. E., Pendleton, R. M., Chick, J. H. and Casper, A. F.** (2016). Long-term changes in fish community structure in relation to the establishment of Asian carps in a large floodplain river. *Biol. Invasions* **18**, 2883-2895.
- Zhang, H., Rutherford, E. S., Mason, D. M., Breck, J. T., Wittmann, M. E., Cooke, R. M., Lodge, D. M., Rothlisberger, J. D., Zhu, X. and Johnson, T. B.** (2016). Forecasting the impacts of silver and bighead carp on the Lake Erie food web. *Trans. Am. Fish. Soc.* **145**, 136-162.
- Zhou, Q., Xie, P., Xu, J., Ke, Z. and Guo, L.** (2009). Growth and food availability of silver and bighead carps: evidence from stable isotope and gut content analysis. *Aquat. Res.* **40**, 1616-1625.